ASME Journal of Biomechanical Engineering
Online journal at:
https://asmedigitalcollection.asme.org/biomechanical

Mohammad Robiul Hossan[1]
ASME Mem.
School of Engineering,
Center for Interdisciplinary Biomedical Education
and Research (CIBER),
University of Central Oklahoma,
Edmond, OK 73034
e-mail: mhossan@uco.edu

Vishal Barot
School of Engineering,
University of Central Oklahoma,
Edmond, OK 73034
e-mail: Vbarot@uco.edu

Seth Harriet
School of Engineering,
University of Central Oklahoma,
Edmond, OK 73034
e-mail: sharriet@uco.edu

Lauren Peters
School of Engineering,
University of Central Oklahoma,
Edmond, OK 73034
e-mail: lpeters6@uco.edu

Alex Christopher Matsayko
School of Engineering,
University of Central Oklahoma,
Edmond, OK 73034
e-mail: amatsayko@uco.edu

Andrew Bauer
Department of Neurosurgery,
University of Oklahoma - Health Science Center,
Oklahoma City, OK 73104
e-mail: andrew-bauer@ouhsc.edu

Khalid Hossain
JP Analytical LLC,
411 Wandering Way,
Ardmore, OK 73401
e-mail: khalid@jpanalytical.com

Engineering Analysis of Non-Braided Polycaprolactone Bioresorbable Flow Diverters for Aneurysms

This paper reports a nonbraided, bioresorbable polycaprolactone (PCL) flow diverter (FD) for the endovascular treatment of aneurysms. Bioresorbable FDs can reduce the risk associated with the permanent metallic FDs as they are resorbed by the body after curing of aneurysms. PCL FDs were designed and fabricated using an in-house hybrid electromelt spinning-fused deposition fabrication unit. Flow diverter's properties, surface qualities, and mechanical characteristics of PCL FDs of 50%, 60%, and 70% porosities were studied using scanning electron microscope (SEM), atomic force microscopy (AFM), and high precision universal testing machine (UTM). The deployability through a clinically relevant catheter was demonstrated in a PDMS aneurysm model. The angiographic visibility of the developed PCL FDs was evaluated using $BaSO_4$ *and* Bi_2O_3 *coatings of various concentration. The average strut thicknesses were* $74.12 \pm 6.63\ \mu m$, $63.07 \pm 1.26\ \mu m$, *and* $56.82 \pm 2.09\ \mu m$ *for PCL FDs with 50%, 60%, and 70% porosities, respectively. They average pore areas for the 50%, 60% and 70% porosities FDs were* $0.055 \pm 0.0056\ mm^2$, $0.\ 0605 \pm 0.0065\ mm^2$, *and* $0.0712 \pm 0.012\ mm^2$, *respectively. The surface quality was great with an RMS roughness value of 14.45 nm. The tensile, radial strength, and flexibility were found to be satisfactory and comparable to the nonbraided coronary stents. The developed PCL FDs were highly flexible and demonstrated to be deployable through conventional delivery system as low as 4 Fr catheters in a PDMS aneurysm model. The visibility under X-ray increases with the increasing concentration of coating materials* $BaSO_4$ *and* Bi_2O_3*. The visibility intensity was slightly higher with* Bi_2O_3 *coating of PCL FDs. The overall results of the engineering analysis of the developed nonbraided PCL FDs are promising.* [DOI: 10.1115/1.4063001]

Keywords: flow diverters, bioresorbable, polycaprolactone (PCL), aneurysms, endovascular treatment

Introduction

Intracranial aneurysm (IA) is a cerebrovascular disorder that begins with a bulge formation on the blood vessel in the brain. If it is undiagnosed and untreated, this bulge can balloon out beyond control and eventually rupture. The rupture of aneurysm causes bleeding in the brain called subarachnoid hemorrhage, which is associated with high mortality rates and significantly impacts the quality of life of the survived patients [1]. Recently, the flow diverting device, a densely meshed braided cylindrical tube, has become an efficient endovascular treatment method for the IA [2]. Upon approval from the federal drug administration (FDA) for the first time in 2011, and later in 2018 as third generation FDs, flow diversion is now an established treatment methods for both giant and small aneurysms [3]. Flow diverters regulate blood flow away from the aneurysm cavity and cause hemostasis for inducing intra-aneurysmal thrombosis [4]. FDs also serve as scaffold for endothelization and finally cure aneurysm by complete occlusions

---

[1] Corresponding author.

Manuscript received January 30, 2023; final manuscript received July 7, 2023; published online August 8, 2023. Assoc. Editor: Katherine Yanhang Zhang.

[4]. Numerous reports and metanalysis have confirmed the efficacy and success of the use of FDs as an endovascular treatment for curing aneurysms [5].

Despite the success of the FDs in curing aneurysms, clinical complications such as late thrombosis, incomplete occlusion, rupture of aneurysms, in-stent stenosis have still been reported in 7% to 10% of patients [6,7]. Many of these complications are attributed to the mechanical properties and structure of the FDs [6,8]. Current FDs are made by braiding metallic microwires that can slide on each other and are susceptible to inconsistency and distorted pore structures [8,9]. This self-expanding FD can cause low-grade constant inflammation due to micromovement, dislodgment, and sliding of the unhinged microwires over the vascular walls [7]. The placement of metallic FDs is irreversible and permanent in the body even after complete cure of aneurysm and remodeling of the blood vessel. This causes a life-long risk for in-stent stenosis and very late thrombosis. For instances, Sleiman et al. reported a very late in-stent thrombosis occurrence in a 78 year old male patient 12 years after implantation of a metal drug eluting stent [10]. In addition, the placement of metal FDs limits future noninvasive electromagnetic field-based diagnosis, such as MRI and X-ray, natural arterial growth and procedures [8]. However, based on the clinical data, the average time period for complete occlusion of aneurysm using FDs is between 6 and 12 months [3,4]. Hence, an ideal flow diverter would be the one that will disappear after completion of aneurysm occlusion and remodeling of the blood vessel.

There are many bioresorbable biomaterials available with degradation rates low enough to withstand more than a year or more in in vivo physiological conditions [11]. Implants and grafts based on these biodegradable biomaterials have been reported in various applications such as in orthopedics, coronary, vascular, and oral/maxillofacial implants [11,12]. Bioresorbable implants eliminate the drawbacks and complications associated with the permanent and metal implants in various clinical applications. For instance, continuous low-grade inflammation, internal injuries and clotting, restenosis, late thrombosis, dislodgment and micromovement of the implants, obstruction of future reintervention, and interference of electromagnetic noninvasive diagnostics were reported to be associated with the metal implants [12,13]. However, there are only a few studies on the development of bioresorbable flow diverters for endovascular treatment of aneurysms. Wang et al. reported a partially bioresorbable FD by combining metallic microwires and biodegradable polyglycolic acid microwires with a 1:1 ratio in 2013 [14]. In 2019, Nishi et al. published their pilot study of poly-L-lactic acid (PLLA) based fully biodegradable flow diverters [15]. They studied the static in vitro degradation rate at regular and elevated temperatures, and the performance of FD was evaluated with rabbit aneurysm model by morphological and histological analysis. Recently, Mitha and his group studied mechanical and thrombogenic characteristics of biodegradable PLLA flow diverters in vitro and using animal model [16]. In the aforementioned studies, the fully bioresorbable FDs were braided and based on PLLA. Though PLLA is a good candidate biomaterial, the acidic degraded constitutes from PLLA can cause vessel inflammatory response and limits its application as FD [17].

Braided FDs are highly flexible, easy to make, and inexpensive [18]. However, braiding has limited controllable parameters in their pore designs and shapes and can suffer from structural distortion as wires can slide on each other [19]. Recently, our group proposed a nonbraided, polycaprolactone (PCL) bioresorbable flow diverter [20]. PCL is a FDA approved biomaterial for biomedical application that takes 2–4 years for complete degradation [21]. Various studies and biomedical applications of PCL as vascular graft, bone implants, suture, dentistry application, and neuroscaffolds are reported in the literature [22,23]. The homogenous and two-stage degradation characteristics, uptake in phagosomes of microphage, and within cells, and excellent mechanical properties of PCL make it a perfect candidate biomaterial for the bioresorbable flow diverters [24]. This paper presents a novel nonbraided bioresorbable PCL flow diverter with associate fabrication methods and engineering analysis. This novel hybrid fabrication method combines the fused deposition modeling technique with electromelt spinning technology to design and fabricate nonbraided flow diverters. Mechanical characterization, feasibility of the deployment through conventional flow diverter delivery catheters, and visibility under angiogram were studied and analyzed for three different porosities of the developed PCL nonbraided FDs.

Materials and Methods

Design and Fabrication. Bioresorbable PCL FDs were made using a custom, in-house and patent pending fabrication unit. The unit consists of a micromotion platform (Newport Corporation, Irvine, CA) with three degrees-of-freedom (x, y, and z movement), electromelt needle, temperature sensors, stepper motors with custom mounting chuck, motor drivers, Arduino control boards, cooling fan, power supplies, and three-dimensional (3D) printed rotary arms. The schematic of the fabrication unit is shown in Fig. 1(*a*), while Fig. 1(*b*) shows the actual setup. The unit combines fused deposition extrusion system with the electromelt spinning technique to fabricate desired flow diverters. Python and C codes were written to achieve a specific porosity, diameter, and length for the PCL flow diverters. The code was uploaded to the hardware using Arduino IDE and a serial communication terminal from a windows machine to Newport's motor control board. The extrusion rate of medical grade PCL 1.75 mm filament, temperature, and spinning rate of the rotary arm was controlled by an Arduino controller. The translation motion of the rotary arm was controlled by the Newport platform motion controller. The porosity and strut thickness of the flow diverters were adjusted by controlling spinning rate, translational motion of the rotary arm, extrusion rate, and electromelt temperature. The PCL flow diverter was fabricated on the rotary arm, removed, and readied for use and further analysis.

Flow Diverter/Surface Characterization. The quality of the fabricated PCL FDs, pore sizes, shapes, porosities, pore densities, and strut thickness was evaluated with visual inspection and under the scanning electron microscope (SEM) at various magnifications. SEM images were imported into the image analysis software IMAGEJ (ImageJ software, NIH), and thresholds were set contrasting the light-colored PCL and the dark color background. Calculations were made based on a calibrated pixel analysis. The light and dark areas are compared in the frame to achieve the measurements for porosity and pore density. The strut thickness is calculated using the pixels in a calibrated length reference in the SEM image. Macros allow for automation for large scale file calculations. Surface roughness and surface quality were evaluated with atomic force microscopy (AFM) using a Digital Instruments Veeco Dimension Edge (Bruker Corporation, Billerica, MA). AFM was in tapping mode. The scan size area was 2 μm X 2 μm with a 256 resolution at a speed of 0.5 Hz. Flow diverters were also loaded into a 0.8 mm diameter delivery catheter and delivered into a PDMS aneurysm model with an inner vessel diameter of 3 mm.

Mechanical Testing. Tensile and longitudinal radial compression of the PCL FDs were conducted using a high precision universal testing machine (The Uni-Vert, Cellscale Inc., Toronto, ON, Canada) with a 5 N load cell and ±0.001 N resolution in room temperature. The special fixture for tensile test was designed and 3D fabricated using commercial PLA filament. PCL FDs were confined vertically to the fixtures using metallic pins as shown in Fig. 1(*c*). The distance between the pins was considered as the effective length of the flow diverters and utilized for the force versus displacement data analysis. The longitudinal radial compression was conducted by compressing about 90% of the nominal diameter of the PCL FDs in the lateral direction of the FDs between flat plates as shown in Fig. 1(*d*). The speed of displacement was set to 0.5 mm/s, and the data collection speed was to 15 Hz or 30 data points collection per mm of

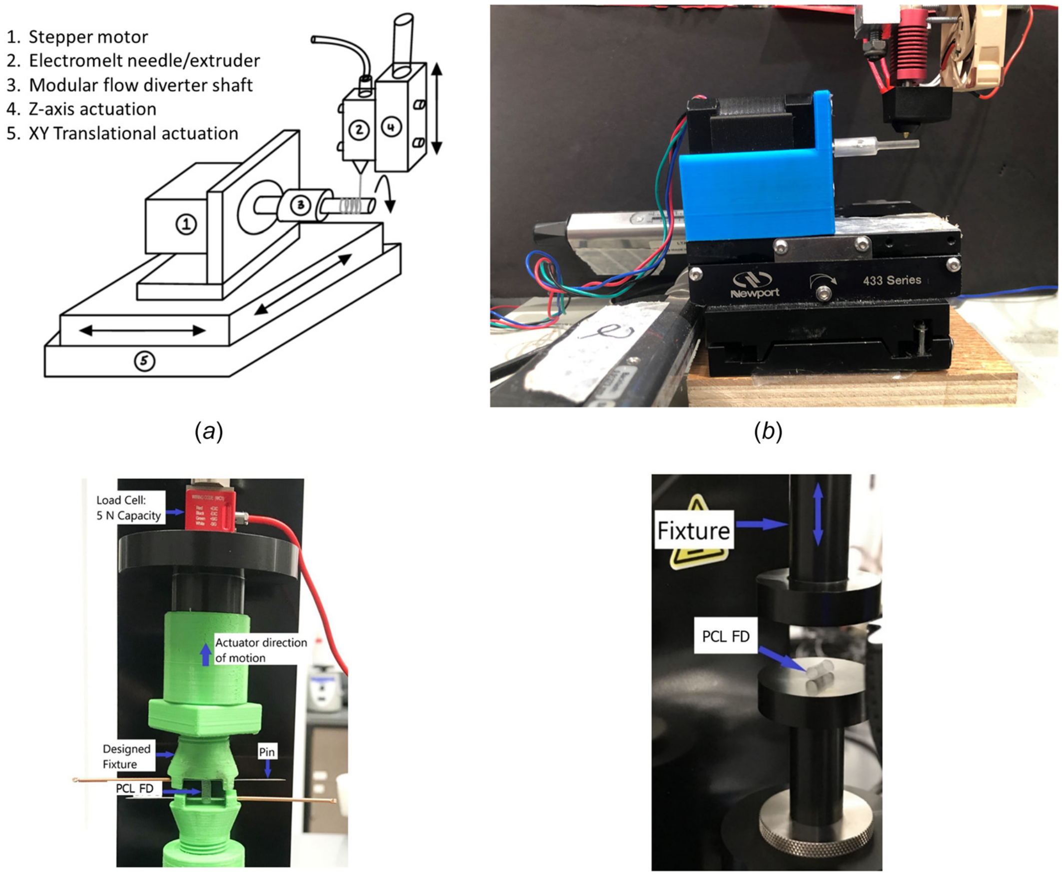

(*a*) (*b*)

(*c*) (*d*)

Fig. 1 (*a*) Schematic of the bioresorbable flow diverter fabrication unit, (*b*) the actual setup, (*c*) tensile test setup where PCL FDs are fixed in the fixture through two pins at the ends of the FDs, and (*d*) longitudinal radial compression setup where PCL FD is compressed in the lateral direction between flat plates

displacement. The nominal diameters of the all PCL FDs for the mechanical testing were 3 mm (±0.2 mm) and lengths were 10 mm (±0.5 mm). For both tensile and longitudinal radial compression tests, three different samples from each porosities of PCL FDs were tested for each experiment.

Radiopacity Coating and X-Ray Visibility Analysis. Prewashed square PCL tiles of 7 × 7 mm were fully coated with varying concentrations of $BaSO_4$ and Bi_2O_3 in PCL for evaluating the visibility under X-ray or angiographic imaging. The radiopacity coating pastes were made at four different compositions as 0.3 g/mL, 0.2 g/mL, 0.15 g/mL, and 0.1 g/mL by combining the appropriate amounts of $BaSO_4$ or Bi_2O_3 with 0.5 g PCL in 5 mL of acetone for 30 min using a sonicator probe. The PCL tiles were then coated by dipping into the appropriate mixture and tapped once against a glass slide to remove excess coating. After drying completely, X-ray images were obtained by using a handheld X-ray machine (DX3000, DEXCOWIN, Geumcheon-gu, Korea) with an exposure time of 1.35 s at a 15 cm distance from the sample. The X-ray images were analyzed for the peak intensity using IMAGEJ software. The highest peak intensity paste was used to coat the PCL FDs with three longitudinal stripes with $BaSO_4$ and Bi_2O_3. The coated PCL FDs' visibility under X-ray was verified and reported.

Statistical Analysis. All experiments and measurements were conducted at least three times for statistical analysis and reproducibility of the experiments. The error was expressed in terms of one standard deviation ($\pm 1\sigma$) in the relevant results unless it is mentioned otherwise. The statistical significance was measured using student *t* test with a *p*-value of 0.05 for all analysis.

Results and Discussion

Flow Diverter Characterization. Polycaprolactone flow diverters were designed and fabricated using in-house fabrication unit with three different porosities – 50%, 60%, and 70% for this study as shown with 8× magnification in Fig. 2(*a*). The porosities are varied by adjusting translational motion and spinning rate of the rotary arm. The pores are usually in diamond shapes, and pore sizes are varied based on the overall porosities of the FDs. The typical pore areas and the strut thickness of the all three porosities are shown in Figs. 2(*b*)–2(*d*). The average pore areas, pore densities, and strut thicknesses are shown in Fig. 3(*a*). The overall pore sizes increase as the porosities increase. They average pore areas for the 50%, 60%, and 70% porosity FDs are (0.055 ± 0.0056) mm^2, (0. 0605 ± 0.0065) mm^2, and (0.0712 ± 0.012) mm^2, respectively. The strut thickness of the FDs decreases as the porosities increased. In other words, the strut size decreases as the material coverage decreases. Unlike braided FDs, the porosities are dependent on the strut thickness. The average strut thickness for 50% porous FDs is (74.12 ± 6.63) μm while strut thicknesses are (63.07 ± 1.26) μm and (56.82 ± 2.09) μm for 60% and 70% porous FDs, respectively. Compared with the bioresorbable coronary stents, the strut thickness of our PCL FDs is much lower. The average strut thickness of the fully bioresorbable coronary stents are 150 μm or more [25,26]. Hence, in terms of the strut thicknesses, all three porosities of the developed PCL FDs are better compared to the existing coronary

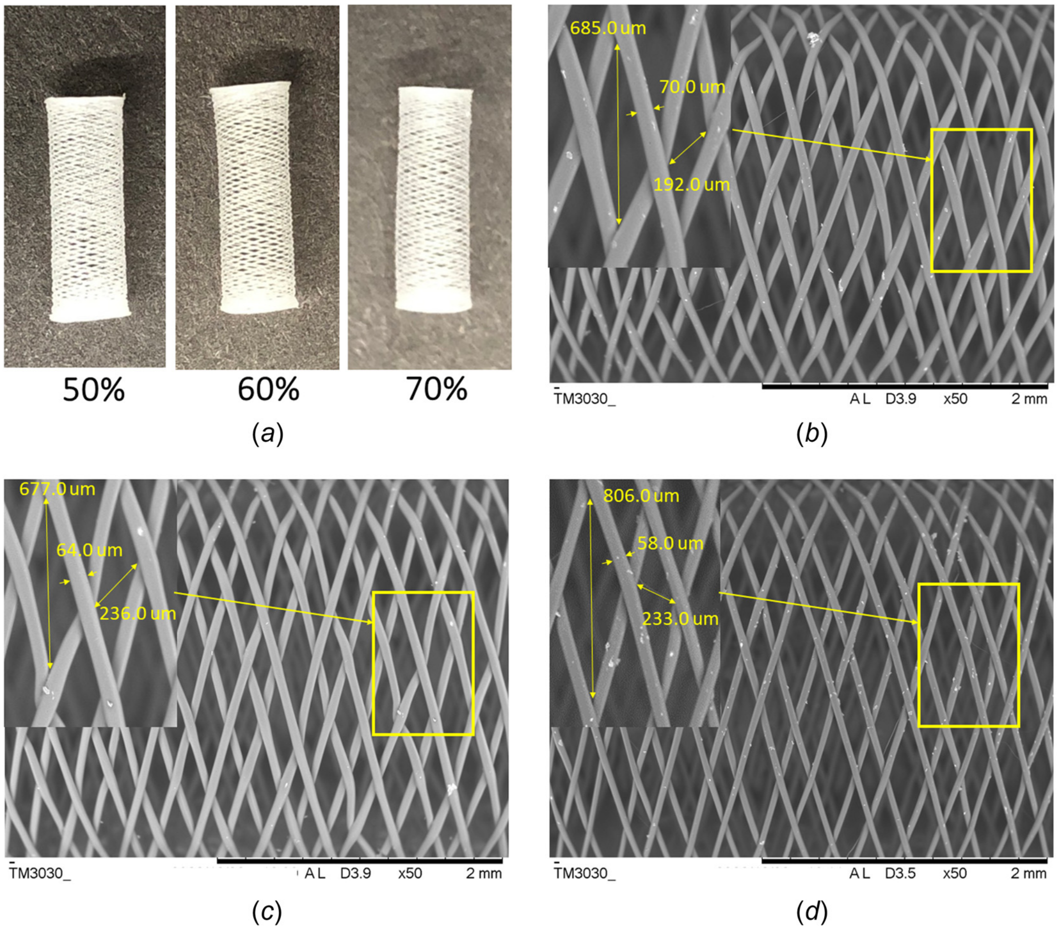

(*a*) (*b*) (*c*) (*d*)

Fig. 2 (*a*) Fabricated bioresorbable nonbraided PCL flow diverters of 50%, 60%, and 70% porosities with 8× magnification; SEM images with typical strut and pore sizes for (*b*) 50% porous, (*c*) 60% porous, and (*d*) 70% porous PCL flow diverters

bioresorbable stents. The thicker strut makes the device stiffer and creates issues in maneuverability and difficulty in the deployment [26]. The smaller thickness of the strut reduces the risk of blood clotting and other complications [26].

The pore densities were also estimated from the SEM images for various FD samples and analyzed for each of the porosities. It is interesting to note that pore densities were found roughly (9 ± 1) pores/mm^2 for all three porosities. Figure 3(*a*) shows the details of the pore densities for all three PCL FD porosities. In conventional braided metallic FDs, the porosities and pore densities are mainly dependent on the number of the microwires and how densely they are braided. Variations in wire diameters, pore densities, and pore areas in the same FDs are not possible. Hence, the controllable parameters in braided FDs are limited. In contrast, the developed nonbraided PCL FDs can have variable porosities, strut thickness, and pore sizes within the same FDs. The occlusion of the blood vessel side branch covered by the FD is a growing concern [27]. Targeted variation in porosities and pore areas can ensure the proper circulation in the side branch. Under visual inspection and SEM images, it confirmed the permanent fusing of the strut in the pores. However, we observed that the quality and strength of the fusion among the strut depends on the cooling rate and extrusion temperature (not shown here). The summary of the flow diverter properties for the developed PCL flow diverters with 50%, 60%, and 70% porosities is shown in Table 1. The surface roughness and overall quality of the strut were also studied under AFM and shown in Figs. 3(*b*)–3(*d*). The surface roughness is about one order higher than the typical glass slide. The typical glass slide roughness value is about 1 nm [28]. The root-mean-square (RMS) roughness value of our PCL FDs was found to be 14.45 nm. The low surface roughness facilitates easier loading and unloading from the catheter delivery system into the aneurysm site [29]. The nanometer scale surface roughness has low friction and easier for delivery [29]. In addition, studies showed that nanometer scale surface roughness in endovascular stents promote endothelization, endothelial and smooth muscle cell adhesion, proliferation, and migration [30]. The nanoscale surface roughness of the coronary stents reduces in-stent stenosis, micromovement of the implant, and late thrombosis [30]. On the other hand, extremely smooth surfaces, such as a glass-like surface of a stent, may cause sliding, micromotion, and dislocations. Dislocation of stents causes severe clinical consequences and require surgical interventions [31,32]. However, higher surface roughness of stents or implants can cause injuries and penetrations on the vascular wall and can lead to the necrosis [33]. Therefore, nanometer scales surface roughness in the developed PCL FDs can have positive impact on the aneurysm treatment.

Tensile Testing of Polycaprolactone Flow Diverters. The results of the tensile test of the PCL flow FDs were shown in Fig. 4. The tensile strength was evaluated based on the ASTM F2942-19 standard for balloon-expandable and self-expanding metallic stents using uni-axial tensile test. The alignment of the specimen PCL FDs at two ends were constantly monitored and checked for each of the tensile test. The misalignment and off-axis tensile test could provide overestimation or underestimation of the tensile test results [34,35]. The misalignment can also alter the failure modes, i.e., tensile failure or shear failure depending on the degree of the misalignments [36]. The tensile force vs percentage of longitudinal elongation is shown in the Figs. 4(*a*)–4(*c*) for the 50%,

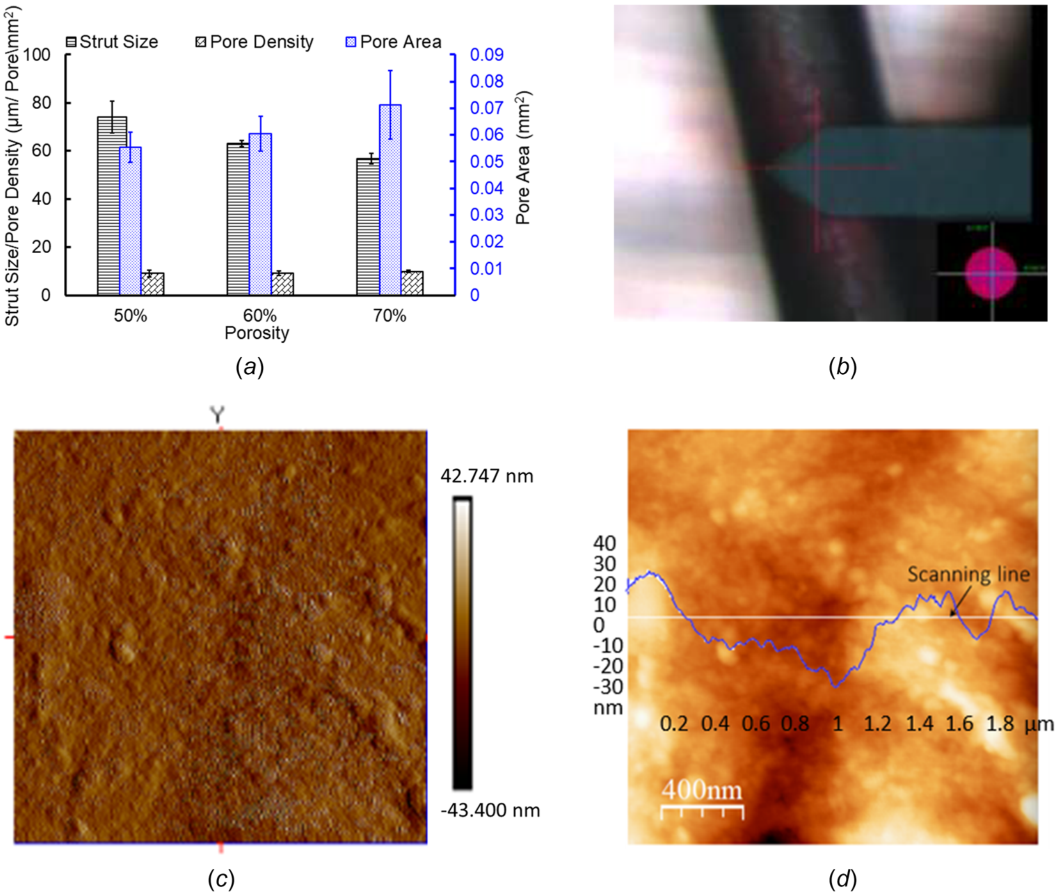

Fig. 3 PCL FD properties and surface characterization (*a*) strut thickness, pore sizes, and pore densities. The error bars are shown as ±1σ standard deviation except for the pore areas, where error bars are shown for 1 standard mean error (SEM), (*b*) optical image showing atomic force microscopy (AFM) probe tip position on a PCL strut on the flow diverter with 40× magnification, (*c*) AFM 3D surface topography of strut surface, and (*d*) variation of surface roughness along the scanning line. The RMS value of surface roughness is 14.45 nm.

60%, and 70% porosities of the FDs, respectively. The percentage elongation was calculated by dividing the displacement value with effective length (δ_t/EL). The overall elongation nature is pretty similar for the all three porosities. However, the required force decreases as material content decreases with the increase of porosities. The load increment was calculated by dividing tensile force with displacement (P_t/δ_t) over each data points and plotted against the percentage of elongation as shown in Figs. 4(*a*)–4(*c*). The best fit curve on the load increment over the elongation can be divided into three stages as demonstrated in the figure. The stage one suggests elastic deformation due to relatively rapid load increment. The stage two indicates the transition from bending to stretching of the struts and strut joints, where struts are connected and formed junctions. The stage three can be interpreted as a typical necking behavior before the failure point and after the ultimate strength or maximum tensile loading point of the network structure. This is interesting to note that the behavior of the PCL flow diverters fairly resembles the typical behavior of the ductile metallic stents [37], though the fundamental mechanism is different. The majority of the pattern in all three stages are similar in PCL FDs with 50% and 60% porosity samples. The load increment drops below the yield point initially before increasing and a relatively short necking during the third stage. However, this is not the case in the results of 70% porosity PCL FD samples suggesting, nonlinearity in structural mechanical properties with larger porosities.

The average maximum tensile forces registered were (1.06 ± 0.036) N, (0.93 ± 0.007) N, and (0.65 ± 0.014) N for PCL FDs with 50%, 60%, and 70% porosities, respectively. The reduction of the average maximum tensile force between PCL FDs with 50% and 60% porosities was 12% or 0.13 N. However, this was as much as 30%, or 0.28 N, between 60% and 70% porosities samples. This may be attributed to the structural variation of the FDs in different porosities and strut architectures. The architectural distortion and structural irregularity of the tows in a braided tube had great impact on its mechanical strength and properties [38,39]. The porosities of the PCL FDs in this report are not just the material contents, and they are also dependent on the strut diameters and junction area sizes as described in the Flow Diverter Characterization section. The local deformation, stress concentration, architectural defects, and failure nature can be quantified and explained by digital image correlation (DIC) analysis [40]. The authors acknowledge the limitation of our current study as it lacks the information of local and dynamic failure behavior of struts and their joints during mechanical testing. However, the presented analysis provides an overall idea of the mechanical and physical properties of the developed PCL bioresorbable flow diverters. Unlike braided FDs, the bioresorbable strut is not sliding on each other. The longitudinal

Table 1 Flow diverter physical properties of three different PCL FDs

PCL FD type	Strut size (μm)	Pore density (pores/mm^2)	Pore area (mm^2)
50% Porosities	74.12 ± 6.63	8.45 ± 1.42	0.055 ± 0.0056
60% Porosities	63.07 ± 1.26	9.26 ± 1.30	0. 0605 ± 0.0065
70% Porosities	56.82 ± 2.09	9.85 ± 0.75	0.0712 ± 0.012

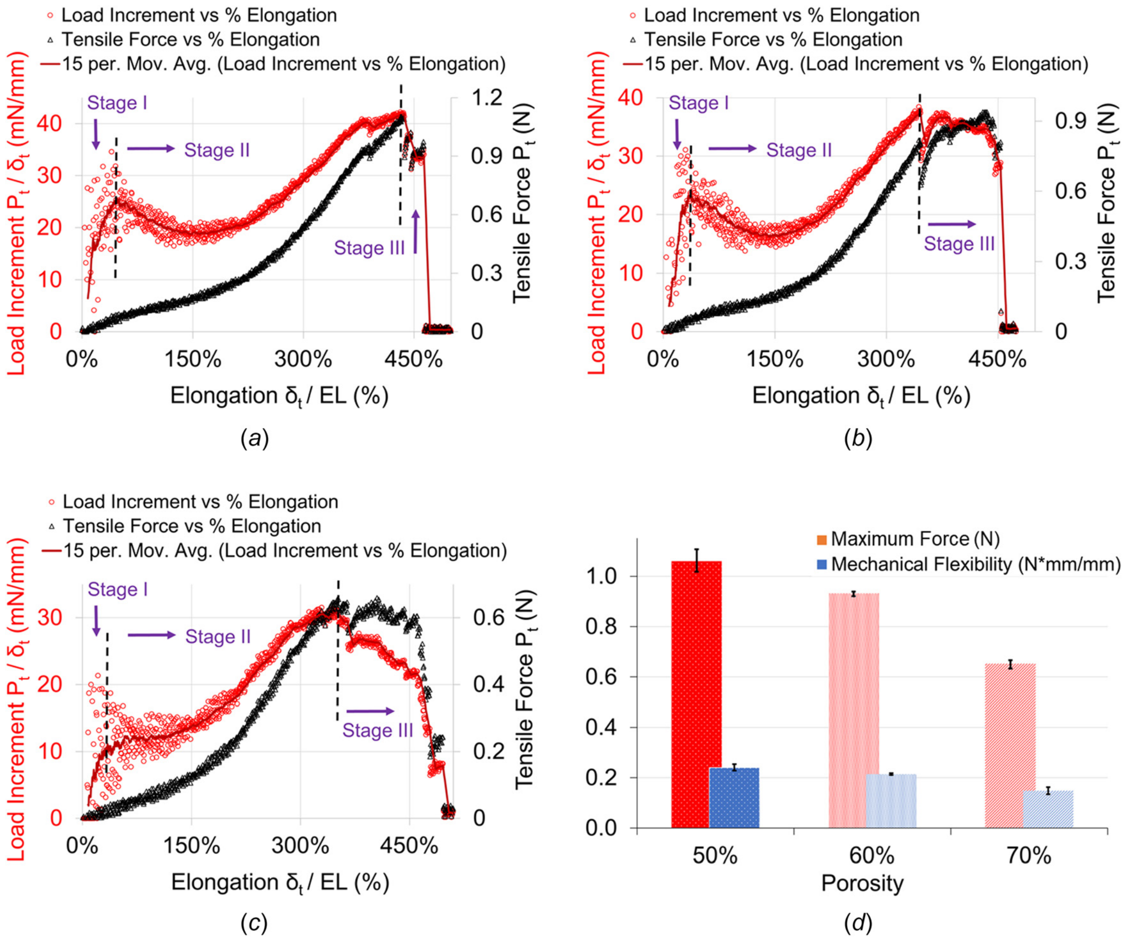

(*a*) (*b*) (*c*) (*d*)

Fig. 4 Tensile test result analysis of PCL nonbraided flow diverters with (*a*) 50%, (*b*) 60%, and (*c*) 70% porosities. (*d*) Tensile test comparison between each porosity. The error bars are shown as $\pm 1\sigma$ standard deviation.

flexibility was also estimated since it is important for loading and unloading in the catheter delivery system, especially for the nonbraided flow diverters. The overall longitudinal mechanical flexibility was calculated using the following equation:

$$\text{Mechancial Flexibility}_{\text{Tensile}} = \frac{P_{\text{t,max}} \cdot \text{EL}}{\delta_{\text{t,max}}} \tag{1}$$

where $P_{\text{t,max}}$ is the maximum tensile force, EL is the effective length of the FDs between the pins, and $\delta_{t,\text{max}}$ is the maximum displacement. The longitudinal mechanical flexibility was found to be (0.24 ± 0.010) N·mm/mm, (0.21 ± 0.003) N·mm/mm, and (0.15 ± 0.011) N·mm/mm for 50%, 60%, and 70% porous PCL FDs, respectively, as shown in Fig. 4(*d*). The more the material's content, i.e., less porous, the more force was required to elongate the FDs, and the less mechanical flexibility.

Radial Compression of Polycaprolactone Flow Diverters. The longitudinal radial compression results for the PCL FDs are shown in Fig. 5. The PCL FDs were compressed about 90% of their original diameter in the lateral direction of the FDs. The percentage lateral compressions of the FDs' inner diameter are plotted against the longitudinal radial force per unit length along with the retraction cycles in Figs. 5(*a*)–5(*c*) for the PCL FDs with 50%, 60%, and 70% porosities, respectively. During the longitudinal compression between flat plates, the PCL FDs formed noncircular cross section and returned to the circular cross section after complete release. The blood vessels are not necessarily uniform. Hence, the average radial force per unit length provides an overall idea about exerted force on the FDs. The percentage lateral compression (DC_{ID}) was obtained using the following equation:

$$\text{DC}_{\text{ID}} = \frac{\delta_{\text{LR}}}{d - 2 \cdot T_W} \tag{2}$$

where δ_{LR} is the longitudinal radial deformation collected as data points during the longitudinal radial compression test, d is the outside diameter, and T_W is the wall thickness of the PCL FDs. The radial load increment became sharply stiff when the lateral compression reached to 50% of its diameter. It showed that the applied radial forces increase as the compression progressed in all porosities. However, higher radial forces are needed to achieve the same compression with higher material contents. In other words, the higher porosities FDs require less force per unit length for the same amount of radial compression. The average maximum radial force per unit length is (101.81 ± 6.12) mN/mm, (73.58 ± 3.83) mN/mm, and (31.42 ± 1.92) mN/mm for about 90% compression to the original diameter of the PCL FDs with 50%, 60% and 70% porosities, respectively. It is also noted that during the retraction cycle, the PCL FDs produce noticeable resistance to the radial compression up to 80% of its original diameter. The normalized radial strength was calculated by normalizing the radial displacement with the FD diameter using the following equation:

$$F_r = \frac{P_{\text{LR}} \cdot d}{\delta_{\text{LR}}} \tag{3}$$

The normalized radial strength is plotted against the radial compression force for each porosity and shown in Figs. 5(*a*)–5(*c*). The slope of the radial strength over the radial force decreases as

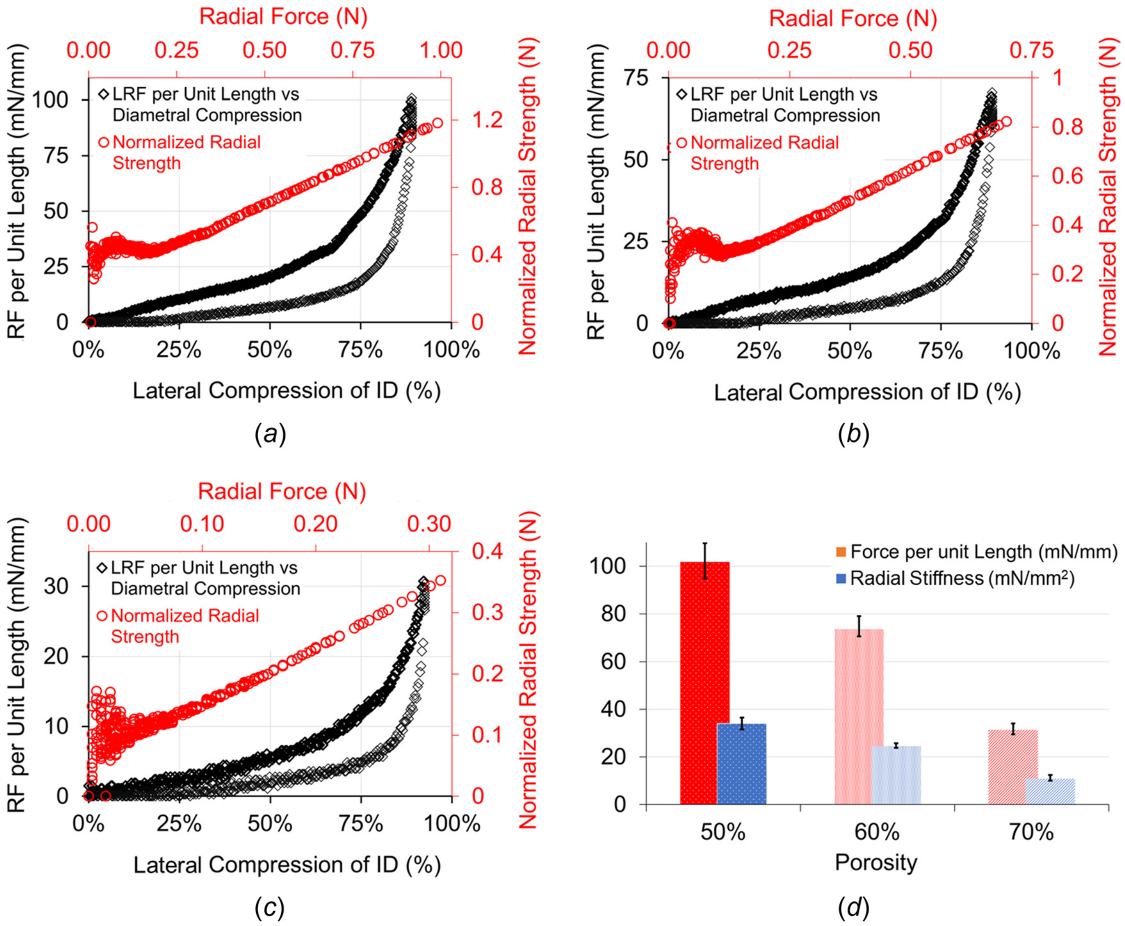

Fig. 5 Radial compression test and analysis for the PCL FDs of porosities (*a*) 50%, (*b*) 60%, (*c*) 70%, and (*d*) comparison among three porosities for the radial force per unit longitudinal length and radial stiffnesses. The error bars are shown as ±1σ standard deviation.

Table 2 Mechanical properties of three different PCL FDs

Test types	50% porosities	60% porosities	70% porosities
Maximum tensile force (N)	1.06 ± 0.036	0.93 ± 0.007	0.65 ± 0.014
Mechanical flexibility (N·mm/mm)	0.24 ± 0.010	0.21 ± 0.003	0.15 ± 0.011
Radial stiffness (mN/mm^2)	34.01 ± 2.02	24.57 ± 0.85	10.85 ± 1.08

porosity increases. However, the radial strength of the developed PCL FDs is dependent on both the material content and the strut sizes. The maximum radial stiffness per unit length of the FDs was derived from the following equation:

$$\text{Maximum radial stiffness} = \frac{P_{\text{LR,max}}}{L \cdot \delta_{\text{LR,max}}} \tag{4}$$

where $P_{\text{LR, max}}$ is the maximum radial force, $\delta_{\text{LR,max}}$ is the maxium radial deformation, and the L is the length of the FD. The maximum radial stiffness per unit length of the PCL FDs was found to be (34.01 ± 2.02) mN/mm^2, (24.57 ± 0.85) mN/mm^2, and (10.85 ± 1.08) mN/mm^2 for FDs with 50%, 60%, and 70% porosities, respectively. The differences in maximum radial stiffness are partially due to the reduction in strut thickness and the reduction of material content in higher porosities of the FDs. The optimum ranges of radial strength and stiffness are important for the successful application of endovascular devices such as stents and flow diverters. Poor radial strength and stiffness of endovascular devices result in poor wall opposition [41]. On the other hand, excessive radial strength and stiffness reduce the flexibility of the device and causes injuries in the vessels [41]. The radial compression results in our devices are comparable to nonbraided endovascular stents reported in the literature [42]. For the ease of reference, the summary of the mechanical characteristics of the developed PCL flow diverters with 50%, 60%, and 70% porosities are shown in Table 2.

Deployability of Polycaprolactone Flow Diverters. The ease of deployability of the developed PCL FDs was studied using various sizes of medical catheters and PDMS aneurysm model as shown in Fig. 6. Unlike braided metallic wired based FDs, the struts in our developed PCL FD are fused together. However, the developed PCL FDs are still very flexible as shown in Fig. 6(*a*). Blood vessels are usually not straight, so the higher bending flexibility is desirable for flow diverters. The developed 3.5 mm nominal diameter PCL FDs were loaded as small as 0.80 mm inner diameter catheter tube

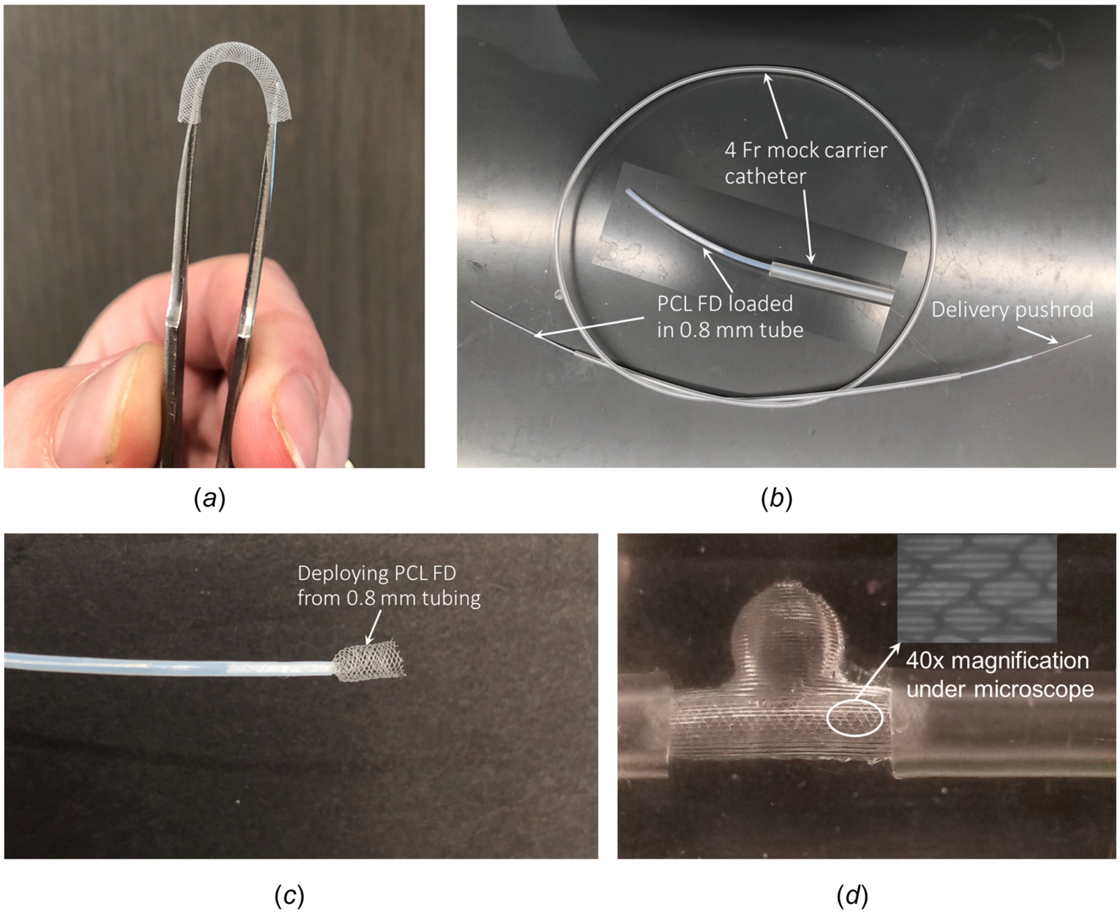

(*a*) (*b*)

(*c*) (*d*)

Fig. 6 (*a*) Bending flexibility demonstration of the PCL FDS, (*b*) 3.5 mm nominal diameter PCL FD is loaded into a 0.8 mm inner diameter tubing and 4 Fr mock carrier catheter, (*c*) deploying form the delivery tube with a half-way deployed PCL FDs from 0.8 mm tubing, and (*d*) Deployed into a 3 mm inner diameter PDMS aneurysm model

without altering the structural integrity. The PCL FDs loaded tubes were demonstrated to run in the mock 4 Fr endovascular carrier catheters (1 Fr. = 0.33 mm). The PCL FD loaded tube in the mock 4 Fr. catheter is shown in Fig. 6(*b*). Like in an endovascular surgery, the loaded PCL FD was deployed from the 0.8 mm tube using a flexible stainless-steel pushrod. A half-deployed PCL FDs from the 0.8 mm tube is shown in Fig. 6(*c*). Upon the delivery from the catheter, the PCL FDs return to about 80% of their original diameter. After deployment from the delivery tube, the strut quality and structural integrity were inspected visually and with SEM. No significant structural damage or tearing of the struts was observed. However, pore sizes and porosities increased about 10 to 15% (not shown) due to stretching during the manual loading process into the catheter tubes. A deployed PCL FD in a transparent PDMS aneurysm model with 3 mm vessel size is shown in Fig. 6(*d*).

Radiopacity Coating and X-Ray Visibility of Polycaprolactone Flow Diverters. Figure 7 shows the radiopacity coating and X-ray visibility studies with the $BaSO_4$ and Bi_2O_3. The results were recorded as average peak intensity in arbitrary units (a.u.). All results are reported with one standard deviation of error. For the $BaSO_4$ samples, the average peak intensities were 112.27 ± 5.06 a.u., 86.25 ± 4.86 a.u., 65.73 ± 8.31 a.u., and 39.58 ± 8.75 a.u. for the 0.3 g/mL, 0.2 g/mL, 0.15 g/mL, and .1 g/mL concentrations, respectively. The average peak intensities for Bi_2O_3 were found to be 124.82 ± 1.19 a.u., 95.16 ± 12.422 a.u., 77.86 ± 2.67 a.u., and 49.94 ± 0.22 a.u. in order of most to least concentrated samples. For both materials, higher concentration was correlated to higher radiopacity. Overall, Bi_2O_3 series had a higher average peak intensity than the $BaSO_4$ series. There was a significant difference in peak intensity between the 0.15 g/mL samples (p-value 0.0376). The 0.3 g/mL, 0.2 g/mL, and 0.1 g/mL concentration samples showed no significant difference between the $BaSO_4$ and Bi_2O_3 coatings.

Placing flow diverters safely in the correct location to treat aneurysms requires them to be detectable by imaging procedures. Barium sulfate is considered a cost-effective and relatively safe compound currently used for imaging the gastrointestinal tract, and in dental devices [43,44]. Other investigations on the cytotoxicity of $BaSO_4$ have found it to be relatively low-toxic, and possibly even promote adhesion of HUVEC cells [20,45]. Bi_2O_3 has also been used to achieve radiopacity in dental devices, and Bi_2O_3 nanoparticles have been used as a contrast agent for imaging procedures [46]. However, it has also been shown that the cytotoxic effect of Bi_2O_3 on HUVEC cells is dependent on concentration [47]. All the radiopaque coating solutions dried quickly, often forming a film on the surface of the coating solution between sample applications. This caused both powders to have a tendency toward clumping, though it appeared slightly more present with the $BaSO_4$ samples. While applying the coatings, it was observed that the .15 g/mL and .1 g/mL samples required more constant mixing for the radiopaque powder to stay evenly dispersed through the PCL-acetone solution. Compared to the higher concentration samples, more of the powder appeared to have settled by the time excess application solution dried. This resulted in a piece of material that was patchy in appearance. Additionally, the 0.15 g/mL Bi_2O_3 solution tended to dry unevenly compared to other samples. Generally, the Bi_2O_3 coatings showed a slightly higher peak intensity than the $BaSO_4$

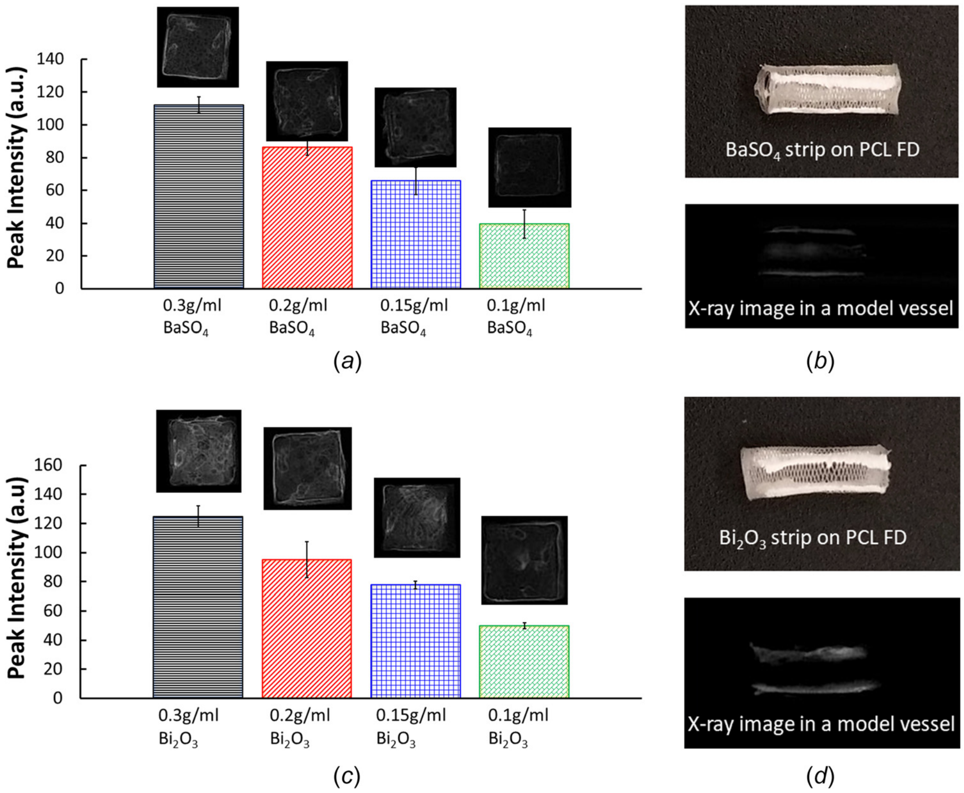

Fig. 7 Radiopacity coating and X-ray image analysis. (*a*) average peak intensity of $BaSO_4$ coated PCL tiles with 4 different concentration, (*b*) $BaSO_4$ strip on the PCL FDs and X-ray image of $BaSO_4$ coated PCL FD in a model vessel, (*c*) average peak intensity of Bi_2O_3 coated PCL tiles with 4 different concentration and (*d*) Bi_2O_3 strip on the PCL FDs and X-ray image of Bi_2O_3 coated PCL FD in a model vessel. The error bars are shown as ±1σ standard deviation.

samples, which is consistent with other findings [48,49]. Overall, the difference in application between the two radiopaque coatings was negligible for the higher concentrations.

Conclusions

This report presents a novel, nonbraided polycaprolactone (PCL) bioresorbable flow diverter for the potential endovascular treatment of aneurysms. PCL is a U.S. FDA approved biomaterials for biomedical applications in human body. To the best of our knowledge, we are the first group who attempted to use PCL in developing nonbraided flow diverters. The physical and mechanical characterizations of PCL FDs with three different porosities are demonstrated. Our in-house fabrication unit is capable of making PCL FDs with various strut thicknesses, pore sizes, pore densities, and porosities. The surface roughness was found to be in nanometer scale ranges that are acceptable and some cases desirable for implants. The tensile and radial compression results are satisfactory and comparable with the nonbraided coronary stents. The bending flexibility, loading, and delivery capability into the desired site using conventional flow diverter delivery catheter system was demonstrated. The visibility under angiographic image of PCL FDs was demonstrated by using two different radiopaque coatings in X-ray images. The overall engineering analysis shows promising results for a potential use of bioresorbable PCL flow diverters for aneurysm treatment. However, further investigation and analysis are needed for the efficacies of PCL FD using animal model and in vitro hemocompatibility, degradation characteristics, and possible design optimization.

Author Contribution Statement

Mohammad R Hossan conceived the idea, formulated PCL FD fabrication unit and design of PCL FDS, analyzed the results, wrote and edited the draft, supervised and lead the overall project. Vishal Barot preformed mechanical testing of PCL FDs, analyzed the results, contributed in the draft writing. Seth Harriet contributed in the PCL FD fabrication unit, designs of PCL, performed PCL FDs characterization, and studied loading and unloading of PCL FDs in the delivery systems. Lauren Peters performed $BaSO_4$ and Bi_2O_3 coating experiment, X-ray imaging, analyzed and contributed in writing the draft and edited. Alex Christopher Matsayko fabricated PCL FDs, contributed in the design and fabrication unit. Andrew Bauer contributed in refining PCL FD design for deployability through catheter systems, clinical aspects of the PCL FD and collaborated in the project. Khalid Hossain preformed surface characterization experiment and helped analyzing the results.

Acknowledgment

Authors thank and acknowledge Steven Long and Zebulon Jandt at the University of Central Oklahoma for their helpful feedbacks and suggestions on flow diverters' fabrication.

Funding Data

- This project was supported by the National Institute of General Medical Sciences of the National Institutes of Health (NIH) under Award No. P20GM103447. Authors also appreciate and acknowledge funding support from the Office of Research and Sponsored programs, the College of Mathematics and Science CURE-STEM program and the office of high impact practices at the University of Central Oklahoma.

Conflicts of Interest

The authors declare no conflicts of interest.

Data Availability Statement

The datasets generated and supporting the findings of this article are obtainable from the corresponding author upon reasonable request.

Nomenclature

d = the outside diameter of the PCL FDs
$\mathrm{DC}_{\mathrm{ID}}$ = the percentage diametral compression
EL = the effective length of the FDs between the pins
F_r = the normalized radial strength
$P_{t,\max}$ = the maximum tensile force
T_W = the wall thickness of the PCL FDs
$\delta_{t,\max}$ = the maximum displacement
δ_{LR} = the longitudinal radial deformation of the PCL FDs
$P_{\mathrm{LR},\max}$ = the maximum radial force
$\delta_{\mathrm{LR},\max}$ = the maximum radial deformation

References

[1] Nieuwkamp, D. J., Setz, L. E., Algra, A., Linn, F. H., de Rooij, N. K., and Rinkel, G. J. E., 2009, "Changes in Case Fatality of Aneurysmal Subarachnoid Haemorrhage Over Time, According to Age, Sex, and Region: A Meta-Analysis," Lancet Neurol., **8**(7), pp. 635–642.

[2] D'Urso, P. I., Lanzino, G., Cloft, H. J., and Kallmes, D. F. K., 2011, "Flow Diversion for Intracranial Aneurysms: a Review," Stroke, **42**(8), pp. 2363–2368.

[3] Shin, D.-S., Carroll, C. P., Elghareeb, M., Hoh, B. L., and Kim, B.-T., 2020, "The Evolution of Flow-Diverting Stents for Cerebral Aneurysms; Historical Review, Modern Application, Complications, and Future Direction," J. Korean Neurosurg. Soc., **63**(2), pp. 137–152.

[4] Ravindran, K., Casabella, A. M., Cebral, J., Brinjikji, W., Kallmes, D. F., and Kadirvel, R. J. N., 2020, "Mechanism of Action and Biology of Flow Diverters in the Treatment of Intracranial Aneurysms," Neurosurg., **86**(Suppl_1), pp. S13–S19.

[5] Brinjikji, W., Murad, M. H., Lanzino, G., Cloft, H. J., and Kallmes, D. F., 2013, "Endovascular Treatment of Intracranial Aneurysms With Flow Diverters: A Meta-Analysis," Stroke, **44**(2), pp. 442–447.

[6] Zhou, G., Su, M., Yin, Y.-L., and Li, M.-H., 2017, "Complications Associated With the Use of Flow-Diverting Devices for Cerebral Aneurysms: A Systematic Review and Meta-Analysis," J. Neurosurg. **42**(6), p. E17.

[7] Aydin, K., Barburoglu, M., Sencer, S., Berdikhojayev, M., Coskun, B., and Akpek, S., 2017, "Flow Diversion With Low-Profile Braided Stents for the Treatment of Very Small or Uncoilable Intracranial Aneurysms at or Distal to the Circle of Willis," Amer. J. Neurorad., **38**(11), pp. 2131–2137.

[8] Zhu, Y., Zhang, H., Zhang, Y., Wu, H., Wei, L., Zhou, G., Zhang, Y., Deng, L., Cheng, Y., Li, M., Santos, H. A., and Cui, W., 2019, "Endovascular Metal Devices for the Treatment of Cerebrovascular Diseases," Adv. Mater., **31**(8), p. 1805452.

[9] Estrade, L., Makoyeva, A., Darsaut, T. E., Ghostine, J., Kouznetsov, E., Salazkin, I., Roy, D., Weill, A., and Raymond, J., 2013, "In Vitro Reproduction of Device Deformation Leading to Thrombotic Complications and Failure of Flow Diversion," Interv. Neuroradiol., **19**(4), pp. 432–437.

[10] Sleiman, E., Tabet, R., Karam, B., Ayad, D., and Royzman, R. J. C., 2020, "Extremely Late-Stent Thromb. 12 Years after Implantation a Drug-Eluting Stent," Cureus, **12**(7), p. e9053.

[11] Treiser, M., Abramson, S., Langer, R., and Kohn, J., 2013, *Degradable and Resorbable Biomaterials, Biomaterials Science: An Introduction to Materials*, 3rd ed., Elsevier Inc., San Diego, CA, pp. 179–195.

[12] Li, C., Guo, C., Fitzpatrick, V., Ibrahim, A., Zwierstra, M. J., Hanna, P., Lechtig, A., et al., 2019, "Design of Biodegradable, Implantable Devices Towards Clinical Translation," Nat. Rev. Materials, **5**(1), pp. 61–81.

[13] Zong, J., He, Q., Liu, Y., Qiu, M., Wu, J., and Hu, B. J. M. T. B., 2022, "Advances in the Development of Biodegradable Coronary Stents: A Translational Perspective," Mater. Today Bio., **19**(16), p. 100368.

[14] Wang, K., Yuan, S., Zhang, X., Liu, Q., Zhong, Q., Zhang, R., Lu, P., and Li, J., 2013, "Biodegradable Flow-Diverting Device for the Treatment of Intracranial Aneurysm: Short-Term Results of a Rabbit Experiment," Neuroradiology, **55**(5), pp. 621–628.

[15] Nishi, H., Ishii, A., Ono, I., Abekura, Y., Ikeda, H., Arai, D., Yamao, Y., et al., 2019, "Biodegradable Flow Diverter for the Treatment of Intracranial Aneurysms: A Pilot Study Using a Rabbit Aneurysm Model," J. Am. Heart Assoc., **8**(20), p. e014074.

[16] Jamshidi, M., Rajabian, M., Avery, M. B., Sundararaj, U., Ronsky, J., Belanger, B., Wong, J. H., et al., 2020, "A Novel Self-Expanding Primarily Bioabsorbable Braided Flow-Diverting Stent for Aneurysms: Initial Safety Results," J. Neurointerv. Surg., **12**(7), pp. 700–705.

[17] Onuma, Y., and Serruys, P. W., 2011, "Bioresorbable Scaffold: The Advent of a New Era in Percutaneous Coronary and Peripheral Revascularization?," Circulation, **123**(7), pp. 779–797.

[18] Kassab, E., Marquardt, A., Neelakantan, L., Frotscher, M., Schreiber, F., Gries, T., Jockenhoevel, S., Gomes, J., and Eggeler, G., 2014, "On the Electropolishing of NiTi Braided Stents–Challenges and Solutions: Über Das Elektropolieren Von Geflochtenen NiTi-Stents–Herausforderungen Und Lösungen," Materialwissenschaft und Werkstofftechnik, **45**(10), pp. 920–929.

[19] Zou, Q., Xue, W., Lin, J., Fu, Y., Guan, G., Wang, F., and Wang, L., 2016, "Mechanical Characteristics of Novel Polyester/NiTi Wires Braided Composite Stent for the Medical Application," Results Phys., **6**, pp. 440–446.

[20] Tidwell, K., Harriet, S., Barot, V., Bauer, A., Vaughan, M. B., and Hossan, M. R., 2021, "Design and Analysis of a Biodegradable Polycaprolactone Flow Diverting Stent for Brain Aneurysms," Bioengineering, **8**(11), p. 183.

[21] Woodruff, M. A., and Hutmacher, D. W., 2010, "The Return of a Forgotten Polymer—Polycaprolactone in the 21st Century," Prog. Polymer Sci., **35**(10), pp. 1217–1256.

[22] Malikmammadov, E., Tanir, T. E., Kiziltay, A., Hasirci, V., and Hasirci, N., 2018, "PCL and PCL-Based Materials in Biomedical Applications," J. Biomater. Sci. Polym. Ed., **29**(7–9), pp. 863–893.

[23] Nga, V. D. W., Lim, J., Choy, D. K. S., Nyein, M. A., Lu, J., Chou, N., Yeo, T. T., et al., 2015, "Effects of Polycaprolactone-Based Scaffolds on the Blood–Brain Barrier and Cerebral Inflammation," Tissue Eng. Part A **21**(3–4), pp. 647–653.

[24] Sun, H., Mei, L., Song, C., Cui, X., and Wang, P. J. B., 2006, "The In Vivo Degradation, Absorption and Excretion of PCL-Based Implant," Biomaterials **27**(9), pp. 1735–1740.

[25] Ormiston, J. A., and Serruys, P. W., 2009, "Bioabsorbable Coronary Stents," Circ.: Cardiovasc. Interventions, **2**(3), pp. 255–260.

[26] Ang, H. Y., Bulluck, H., Wong, P., Venkatraman, S. S., Huang, Y., and Foin, N., 2017, "Bioresorbable Stents: Current and Upcoming Bioresorbable Technologies," Int. J. Cardiol., **228**, pp. 931–939.

[27] Bhogal, P., Ganslandt, O., Bäzner, H., Henkes, H., and Pérez, M. A., 2017, "The Fate of Side Branches Covered by Flow Diverters–Results From 140 Patients," World Neurosurg., **103**, pp. 789–798.

[28] Rush, M. N., Brambilla, S., Speckart, S., Montaño, G. A., and Brown, M. J., 2018, "Glass-Particle Adhesion-Force-Distribution on Clean (Laboratory) and Contaminated (Outdoor) Surfaces," J. Aerosol Sci. **123**, pp. 231–244.

[29] Nikolsky, E., Gruberg, L., Pechersky, S., Kapeliovich, M., Grenadier, E., Amikam, S., Boulos, M., et al., 2003, "Stent Deployment Failure: Reasons, Implications, and Short-and Long-Term Outcomes," Catheter. Cardiovasc. Interv., **59**(3), pp. 324–328.

[30] Dong, J., Pacella, M., Liu, Y., and Zhao, L., 2022, "Surface Engineering and the Application of Laser-Based Processes to Stents-A Review of the Latest Development," Bioactive Mater., **10**, pp. 159–184.

[31] Diller, R., Senninger, N., Kautz, G., and Tübergen, D., 2003, "Stent Migration Necessitating Surgical Intervention," Surg. Endoscopy, **17**(11), pp. 1803–1807.

[32] Brown, D., Naidu, J., and Thomas, R. T., 2021, "Bowel Perforation: A 'Not so Rare' Complication of Biliary Stent Migration," ANZ J. Surg., **91**(12), pp. E784–E786.

[33] Sheth, S., Litvack, F., Dev, V., Fishbein, M. C., Forrester, J. S., and Eigler, N. J. C., 1996, "Subacute Thrombosis and Vascular Injury Resulting From Slotted-Tube Nitinol and Stainless Steel Stents in a Rabbit Carotid Artery Model," Circulation, **94**(7), pp. 1733–1740.

[34] Love-Baker, C. A., Harrell, T. M., Brown, K. R., Bumgardner, C. H., and Li, X. C., 2021, "Analyzing the Effect of Misalignment on Single-Filament Carbon Fiber Tensile Testing Via Stereoscopic Computer Vision Imaging," Meas. Sci. Technol., **32**(6), p. 065904.

[35] Li, X., Wang, X., Chang, W.-C., Chao, Y. J., and Chang, M. J., 2005, "Effect of Tensile Offset Angles on Micro/Nanoscale Tensile Testing," Rev. Sci. Instrum., **76**(3), p. 033904.

[36] Harrell, T. M., Love-Baker, C., Brown, K. R., Bumgardner, C. H., and Li, X., 2022, "Extracting Single Fiber Transverse and Shear Moduli From Off-Axis Misalignment Fiber Tensile Testing," Composites, Part A, **163**, p. 107204.

[37] Yokoo, T., Shimizu, I., Wada, A., Takaki, A., Okada, S., Hatakeyama, M., and Yamashita, S., 2014, "Development of Test Methods for Mechanical Property Evaluation of Balloon-Expandable CoCr Alloy Stent," J. Jap. Soc. Exp. Mech. **14**(Special_Issue), pp. s285–s290.

[38] Heim, F. M., Daspit, J. T., and Li, X. J. C. P. B. E., 2020, "Quantifying the Effect of Tow Architecture Variability on the Performance of Biaxially Braided Composite Tubes," Composites, Part B **201**, p. 108383.

[39] Heim, F. M., Daspit, J. T., Holzmond, O. B., Croom, B. P., and Li, X., 2020, "Analysis of Tow Architecture Variability in Biaxially Braided Composite Tubes," Composites, Part B **190**, p. 107938.

[40] Bumgardner, C. H., Heim, F. M., Roache, D. C., Jarama, A., Xu, P., Lu, R., Lahoda, E. J., et al., 2020, "Unveiling Hermetic Failure of Ceramic Tubes by Digital Image Correlation and Acoustic Emission," J. Am. Ceram. Soc., **103**(3), pp. 2146–2159.

[41] Ma, J., You, Z., Byrne, J., and Rizkallah, R. R., 2014, "Design and Mechanical Properties of a Novel Cerebral Flow Diverter Stent," Ann. Biomed. Eng., **42**(5), pp. 960–970.

[42] Matsumoto, T., Matsubara, Y., Aoyagi, Y., Matsuda, D., Okadome, J., Morisaki, K., Inoue, K., et al., 2016, "Radial Force Measurement of Endovascular Stents: Influence of Stent Design and Diameter," Sage J., **24**(2), pp. 171–176.

[43] Murray, P. E., Lumley, P. J., Ross, H. F., and Smith, A. J., 2000, "Tooth Slice Organ Culture for Cytotoxicity Assessment of Dental Materials," Biomaterials, **21**(16), pp. 1711–1721.

[44] Zaccarini, D. J., Lubin, D., Sanyal, S., and Abraham, J. L., 2022, "Barium Sulfate Deposition in the Gastrointestinal Tract: Review of the Literature," Diagn. Pathol., **17**(1), p. 99.

[45] Lämsä, T., Jin, H., Mikkonen, J., Laukkarinen, J., Sand, J., and Nordback, I., 2006, "Biocompatibility of a New Bioabsorbable Radiopaque Stent Material (Ba SO$_4$ Containing Poly-L,D-Lactide) in the Rat Pancreas," Pancreatology, **6**(4), pp. 301–305.

[46] Bartoli, M., Jagdale, P., and Tagliaferro, A., 2020, "A Short Review on Biomedical Applications of Nanostructured Bismuth Oxide and Related Nanomaterials," Materials, **13**(22), p. 5234.

[47] Sarani, M., Tosan, F., Hasani, S. A., Barani, M., Adeli-Sardou, M., Khosravani, M., Niknam, S., et al., 2022, "Study of In Vitro Cytotoxic Performance of Biosynthesized α-Bi$_2$O$_3$ NPs, Mn-Doped and Zn-Doped Bi$_2$O$_3$ NPs Against MCF-7 and HUVEC Cell Lines," J. Mater. Res. Technol., **19**, pp. 140–150.

[48] Bortoluzzi, E. A., Guerreiro-Tanomaru, J. M., Tanomaru-Filho, M., and Duarte, M. A. H., 2009, "Radiographic Effect of Different Radiopacifiers on a Potential Retrograde Filling Material," Oral Surg., Oral Med., Oral Pathol., Oral Radiol., Endodontol., **108**(4), pp. 628–632.

[49] Chen, Y.-Z., Lü, X.-Y., and Liu, G.-D., 2018, "Effects of Different Radio-Opacifying Agents on Physicochemical and Biological Properties of a Novel Root-End Filling Material," PLoS One, **13**(2), pp. e0191123–e0191123.